Superplastic deformation behaviour and microstructure evolution of near-α Ti-Al-Mn alloy

A.V. Mikhaylovskaya[a,*], A.O. Mosleh[a,b], A.D. Kotov[a,e], J.S. Kwame[d], T. Pourcelot[a,c], I.S. Golovin[a], V.K. Portnoy[a]

[a] National University of Science and Technology "MISiS", Leninsky Prospekt, 4, Moscow 119049, Russian Federation

[b] Shoubra Faculty of Engineering, Benha University, Shoubra St. 108, Shoubra, P.O. 11629, Cairo, Egypt

[c] European School of Engineers and Materials Science of Nancy (EEIGM), Nancy 54000, France

[d] Advanced Forming Research Centre - University of Strathclyde, 85 Inchinnan Dr, Inchinnan, Renfrew PA4 9LJ, United Kingdom

[e] National Research University "Higher School of Economics", Moscow Institute of Electronics and Mathematics, 123458 Tallinskaya 34, Moscow, Russia

Abstract

Superplastic deformation behaviour of conventional sheets of a near-α titanium alloy (Ti-2.5Al-1.8Mn) was studied by a step-by-step decrease of the strain rate and constant strain rate tests in a temperature range of 790–915 °C. The research found that superplastic deformation is possible in a temperature range of 815–890 °C and a constant strain rate range of 2×10^{-4} to 1×10^{-3} s^{-1} with elongation above 300% and m-index above 0.4. Also, the research identified the optimum superplastic temperature range of 815–850 °C and constant strain rate of 4×10^{-4} s^{-1} which provide a maximum elongation of 600–650%. Strain hardening is accelerated by dynamic grain growth at high temperatures of 865 and 890 °C. High dislocation activity is observed at superplastic flow in α-phase. Constitutive modelling of superplastic deformation behaviour is performed, and possible deformation mechanisms are discussed. It is suggested that grain boundary sliding between the α-grains is accommodated by a dislocation slip/creep mechanism.

Keywords: Superplasticity, Titanium alloys, Micro-size grain structure, Dislocation structure

1. Introduction

Application of titanium alloys in aerospace engineering is growing every year [1]. Titanium- based alloys are widely used for superplastic forming (SPF) of complex shape aerospace components [2]. SPF allows saving materials and improving product quality, in particular, they increase strength and reduce final weight of the components [1–3]. A very important advantage of the SPF method is high accuracy of die surface reproduction and a possibility to achieve very complex shape parts, which is

essential for Ti-based alloys due to their poor formability at low temperatures [3]. One of the first studies on superplasticity of titanium was performed on the Ti-5Al-2.5Sn α-type alloy [4]. Subsequent studies found that excellent superplastic properties are observed in α+β type titanium alloys with high volume fraction of the β- phase [2]. The greater part of the literature on superplastic deformation of titanium alloys pay particular attention to α+β type alloys, especially Ti-6Al-4V [2,3,5–8]. At the same time, near-α titanium alloys are also very attractive for airspace applications [1]. Their advantages are as follows: light weight, superior fatigue and creep properties at elevated temperatures, adequate strength, toughness and weldability. As aresult, near-α alloys are extensively used in jet engines. In recent times, studies on superplasticity of near-α alloys have considerably increased [9–18] due to rapidly growing applications of SPF of Ti alloys in airspace engineering. To perform SPF, one needs to understand the superplastic tensile behaviour and microstructure evolution during the deformation of near-α type alloys. Sun and Wan [13] studied the superplasticity of the TA15 alloy with an initial grain size of 2 μm. They showed that the alloy exhibited maximum elongation of 1074% at 900 °C and strain rate of 3.3×10^{-4} s−1. Based on the analysis of the m values, the apparent activation energy and the microstructure evolution, the research demonstrated that the grain boundary sliding in the studied TA15 alloy is accommodated by the grain boundary diffusion at low strain rates and high temperatures; and also by the dislocation glide creep at high strain rates and low temperatures. Lin et al. [15] studied the microstructure and texture evolution of a near-α Ti–6.0Al–1.21Nb–9.04Zr–3.88Sn–1.59W–0.28Si alloy during tensile tests at 900 °C and initial strain rates of 3×10^{-2} and 3×10^{-3} s−1. The authors reported that the principal deformation process was dynamic recrystallisation. It was also found that the dynamic recrystallisation process weakened the initial textures. Another near-α type alloy, Ti-5Al-4Sn-2Zr-1Mo-0.25Si-1Nd, was tensile tested in a temperature range of 885–935 °C and a strain rate range of 8.3×10^{-4} to 1.33×10^{-2} s−1 [16]. It was shown that the dynamic recrystallisation occurs at both primary and steady stages of superplastic deformation and is responsible for the softening effect at a stable flow stage. It was concluded that the main deformation mechanism at the steady stage is grain boundary sliding accommodated by the grain rotation process. Similar effects of superplastic deformation in the near-α Ti-5.3Al-3.5Sn-3.0Zr-1.0Mo-0.4Ta-0.5Nb-0.25Si alloy were observed by Liu et al. [17] and in the (α + β) type alloy observed by Xu et al. [18]. Even though the superplastic deformation behaviour of some near-α titanium alloys has been recently studied, there is not much literature on the superplasticity of the Ti-2.5Al-1.8Mn near-α aerospace alloy. This paper provides a better understanding of the superplasticity phenomena required to perform SPF via a detailed study of the tensile deformation behaviour and the microstructure evolution of Ti-2.5Al- 1.8Mn alloy.

1.1. Material and methods

Conventional sheets of Ti-2.5 wt%Al-1.8 wt%Mn alloy with a thickness of 1.55 mm were analysed. Thermo-calc (database TTTi3) was used to analyse the phase volume fractions and compositions which formed under equilibrium conditions at various temperatures. The as annealed and as-deformed microstructures were studied after water quenching from annealing and deformation temperatures, accordingly. Annealing and deformation processes were performed in argon atmosphere to prevent oxidation of the surface. The samples for the microstructure studies were prepared by mechanical grinding on SiC papers and polishing on colloidal silicon suspension. Subsequent etching by 15%HF+15%HNO3+70%C2H5O8 solution for 5 s was performed. Scanning electron microscopy (SEM) using a TESCANVega 3 fitted with EDS and EBSD techniques were applied for compositions, phases parameters, grain and subgrain size analyses. The EBSD analysis was performed with a step size of 0.4 μm and a scan area of 250×250 μm. Disc-shaped samples with a diameter of 3 mm and a major axis parallel to the deformation direction were used for the transmission electron microscopy (TEM). TEM studies were performed using the JEOL JEM–2000 EX microscope. The discs were electrochemically thinned by twin-jet polishing using Struers Tenupol as the A3 electrolyte at a temperature of (20 ± 1) °C and a voltage of 28 V. Superplastic indicators and mechanical properties at room temperature were determined using a uniaxial tensile test on a Walter − Bay LFM100 test machine with a program service for the in-situ traverse motion. The samples with a gauge section size of 6.0×1.55 mm and a gauge length of 17 mm were cut parallel to the rolling direction. Step by- step decreasing strain rate tests were done to evaluate the temperature, the strain rate ranges of superplasticity and the strain rate sensitivity m-index. The strain rate was decreased 1.5 times in each step in a strain rate range of 1×10^{-2} to 5×10^{-5} s^{-1}. The index m was determined as lns-lne slope in each step. The constant strain rate tests were performed in a temperature range from 790 to 915 °C and a strain rate range of 2×10^{-4} to 1×10^{-3} s^{-1} to determine the elongations to failure, stress values and the strain hardening coefficient n.

2. Experimental results

2.1. Microstructure before start of superplastic deformation

A two-phase structure of α (dark in Fig. 1) and β (bright in Fig. 1) phases is observed in the as-proceeded sample. The initial volume fraction of the β-phase is 6% as calculated by a linear intercept method. Fig. 2a shows the polythermal section of the Ti-Al-Mn phase diagram (Thermo-calc model). The equilibrium polymorphic transformation temperature (β-transus) of the studied composition of Ti-2.5Al-1.8Mn is calculated as 906 °C.
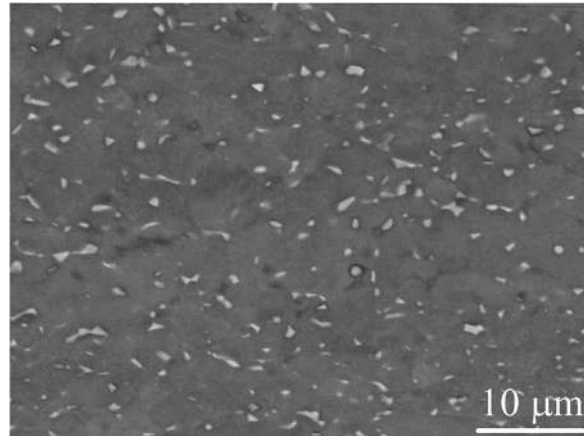
Fig. 1. Initial microstructure of the studied material
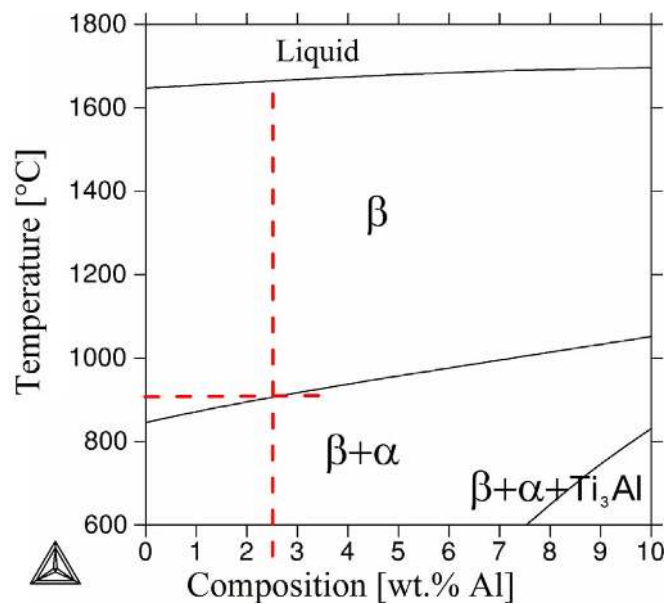

Fig. 2. Polythermic section of the Ti-Mn-Al phase diagram 1.8%Mn (Thermo-Calc, TTTi3 database)

The microstructure studies were performed after 30 min of annealing at the temperature range of 790–915 °C with a step of 25 °C and subsequent water quenching to analyse the grain size and the volume fraction of the α and β-phases before the start of superplastic deformation (Fig. 3). The martensitic plates of α′-phase are observed in the transformed β matrix as a result of the fast cooling at temperatures above 840 °C (Fig. 3d–f). Only coarse transformed β-grains with a size of (300–400) μm consisting of α′ martensite needles are formed after rapid cooling from a high temperature of 915 °C (Fig. 3f). Thus, the temperature of 915 °C belongs to the single β-phase field, which is in agreement with the ThermoCalc data (Fig. 2). The β-phase volume fraction increases with increasing the temperature from 10% at 790 °C to 70% at 890 °C (Fig. 4a). Fine alpha (3.5 μm) and beta (1.5 μm) grains are observed after annealing at 790 and 815 °C (Fig. 4b). The grains of the α-phase slightly grow to 4.7 μm at a high temperature of 890 °C. The average β-grain size increases more than twice− from 1.5 to 3.5 μm− with increasing the temperature from 815 °C to 890 °C (Fig. 4b). The

concentration of Al in both phases and Mn in the α-phase changes insignificantly in the studied temperature range (Fig. 4c). Mn concentration in the β-phase significantly decreases from 5.3 to 1.1 wt%, according to the EDS phase composition analysis and from 7.2 to 2.2 wt%, according to Thermocalc calculation, with increasing the temperature from 790 to 890 °C. It is notable that the equilibrium concentration values (dotted lines in Fig. 4c) and the SEM-EDS data (solid lines in Fig. 4c) are different, which means that the diffusion processes were incomplete at annealing, and the alloy exhibits a non-equilibrium state even at high temperatures.
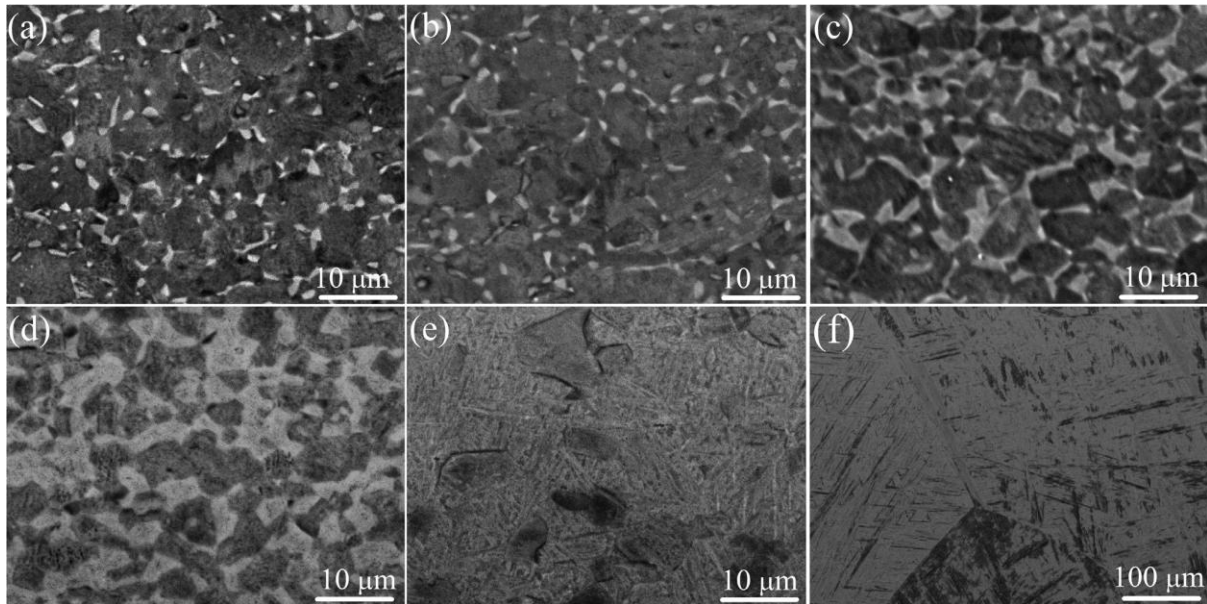

Fig. 3. The microstructure evaluation of the near - α alloy after 30 min of annealing at different temperatures: 790 °C (a), 815 °C (b), 840 °C (c), 865 °C (d), 890 °C (e), 915 °C – (f).

2.2. Superplastic tensile tests

The superplastic behaviour with a sigmoidal shape of the logarithmic stress-strain rate curves (Fig. 5a) and m values above 0.5 (Fig. 5b) are observed at a temperature range of 815–890 °C and a strain rate range of 1×10^{-4}–1×10^{-3} s^{-1}. Superplasticity can be found at 790 °C, though at a very low strain rate range of 1×10^{-4} to 1×10^{-5} s^{-1}. The m-index decreases and exhibits a maximum of 0.35 in the β-phase field at a temperature of 915 °C. The stress values decrease with increasing the temperature from 790 to 890 °C, whereas they increase again at 915 °C due to the formation of coarse β-grains. The constant strain rate tests were performed at strain rates in region II (the linear part of the stress-strain rate curves in Fig. 5a). The stress-strain data at a constant strain rate range of 2×10^{-4} to 1×10^{-3} s^{-1} and a temperature range of 790–915 °C are shown in Fig. 6a–c. The flow stress in most cases decrease with increasing the temperature from 790 to 890 °C and the maximum stress value does not exceed 35 MPa in the studied strain rate and the temperature ranges. Significant strain hardening is observed at elevated temperatures. Thus, the strain hardening coefficient at the steady

stage rises from 0.20 to 0.35 at 2×10^{-4} s^{-1} and from 0.15 to 0.4 at $(4–8) \times 10^{-4}$ s^{-1} in a temperature range of 815–890 °C (Fig. 6d). It should be noted that the tests were performed by maintaining the constant value of the strain rates during the experiment, and there is no decreasing stress values caused by reducing the real strain rate at the initial strain rate tests (tests with constant traverse mouton). Strong strain softening at large strains (1.4–1.8) is a result of necking.
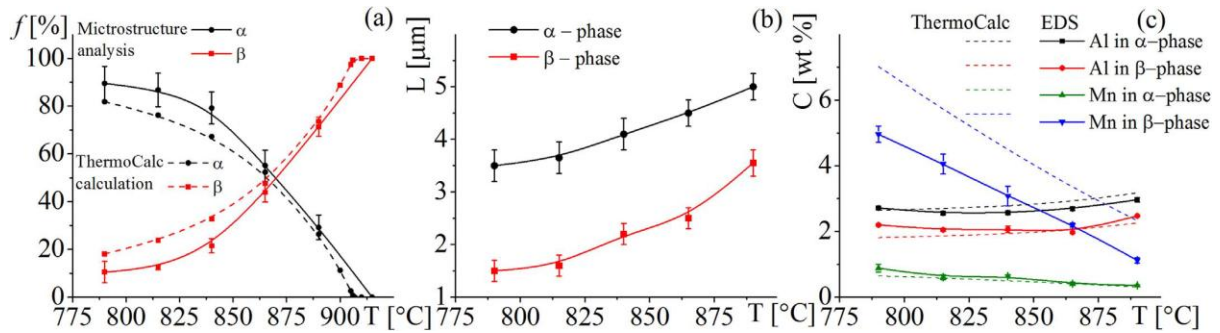

Fig. 4. The volume fraction f (a) and the chemical composition in wt%C (c) of α and β phases through Thermo-Calc calculation (dotted lines), and through the EDS analysis (solid lines) and the grain size, L (b) after 30 min of annealing at various temperatures.

Fig. 6e shows the elongation to failure at different strain rates and temperatures. The transformation of α→ β takes place at ≈ 906 °C, which results in poor superplasticity at 915 °C. Despite the fact that m index is above 0.3, necking and elongation below 200% are observed. Possibly, the ideal superplasticity sigmoidal shape of the stress-strain rate curve in the β-phase field is a result of microstructure evolution (significant grain and subgrain growth) and strong microstructure sensitivity to increase both strain rate and deformation time at elevated temperatures. Low temperature of 790 °C provides a similar poor elongation of 200–280% in the studied strain rate range of 2×10^{-4} to 8×10^{-4} s^{-1}. Elongations above 300% and stress values below 35 MPa, which are suitable for superplastic forming, are observed in a temperature range of 815–890 °C and a strain rate range of 4×10^{-4} to 1×10^{-3} s^{-1}. The maximum elongation of 600–650% is achieved in a temperature range of 815–850 °C and a strain rate value of 4×10^{-4} s^{-1}. The maximum elongation values correspond with the utmost m-values calculated using stress values at the steady stage (e=0.5) in a temperature range of 815–890 °C (Fig. 6f).
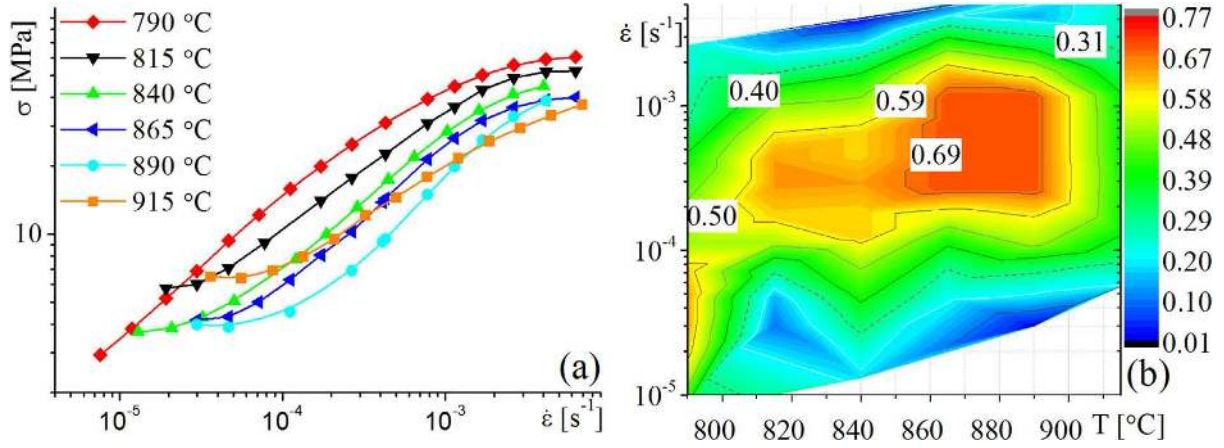
Fig. 5. Stress-strain rate curves (a) and contour of strain rate sensitivity index m vs strain rate and temperature (b).

2.3. Constitutive modelling of deformation behaviour

Superplastic deformation is known to be a diffusion-controlled hot deformation process and the effects of temperatures and strain rate on deformation behaviour could be represented by the Zener-Hollomon parameter (Z) (Eqs. (1) and (2)) [19]. The relationship between Z and the flow stress (σ) can be expressed by different empirical equations (Eq. (3)): the power function (3.1), the exponential function (3.2) and the hyperbolic sine function (3.3) [20]. These relationships are mathematically expressed as:

$$z = \dot{\varepsilon} exp\left(\frac{Q}{RT}\right) \tag{1}$$

$$\dot{\varepsilon} = Af(\sigma)exp\left(-\frac{Q}{RT}\right) \tag{2}$$

$$f(\sigma) = \begin{cases} \sigma^{n_1} & 3.1 \\ exp(\beta\sigma) & 3.2 \\ [sinh(\alpha\sigma)]^{n_2} & 3.3 \end{cases} \tag{3}$$

where $\dot{\varepsilon}$ is the strain rate value (s−1); T is the deformation temperature (K); Q is the effective activation energy of deformation (kJ/mol); and R is the universal gas constant (8.314 kJ mol−1 K−1); A1, A2, A3, n1, n2, β and α are material constants, α is a stress multiplier and a constant which adjusts the predicted values into the right range; α can be described as:

$$\alpha = \frac{\beta}{n_1} \tag{4}$$

The constant value in Eq. (3.1) and Eq. (3.2) were found by plotting the dependencies of ln(Z) vs. ln(σ) and ln(Z) vs. σ, correspondently. The values of α were determined using Eq. (4) and the values

of the unknown constants in Eq. (3.3) were determined by constructing the dependencies of ln(Z) vs ln(sinh(αβ)). The average value of the strain rate sensitivity index m can be calculated as:

$$m = \frac{1}{n_1}$$

(5)

Table 1 shows the calculated values of A1, A2, A3, n1/m, n2, β, Q and α in the temperature range of 815–890 °C and a strain rate range of 1×10^{-4} to 1×10^{-3} s−1. There is no significant difference between the effective activation energy values which were calculated by the above equations, and 184–188 kJ/mol was obtained with an average m-value of 0.67.
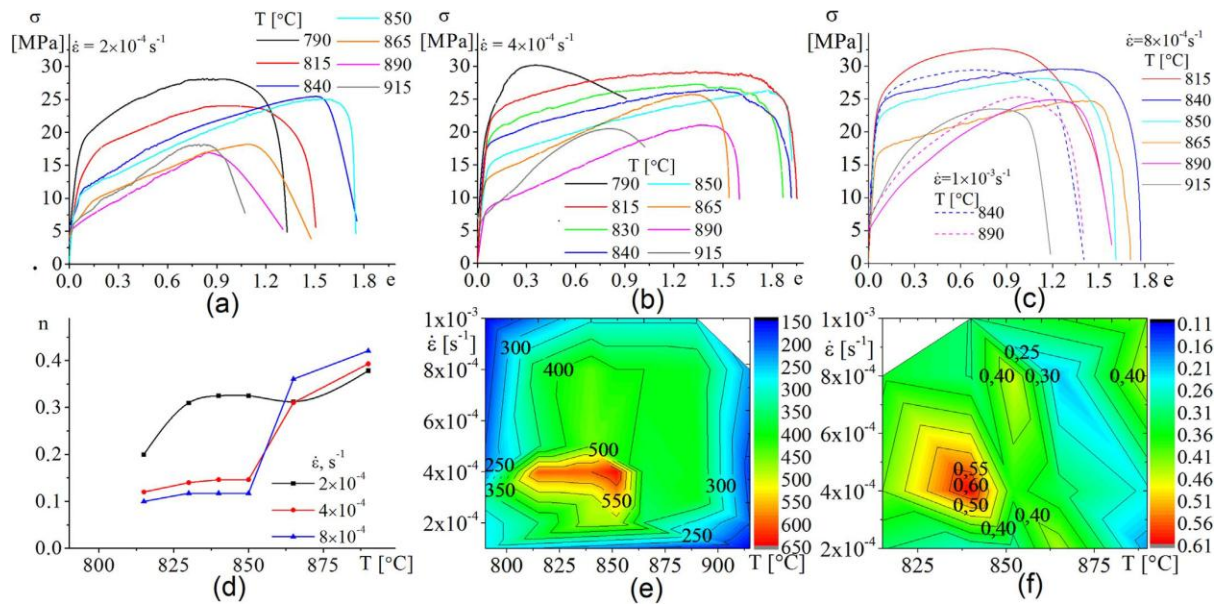

Fig. 6. The constant strain rate tensile tests results: flow stress vs strain at the constant strain rate of 2×10−4 s−1 (a) 4×10−4 s−1 (b), 2×10−4 s−1 (c) and different temperatures and strain hardening coefficient n – vs temperature (d) elongation to failure (e) and strain rate sensitivity exponent for 0.5 strain value (f) maps, as a function of temperature and strain rate.

Table 1. The calculated values for A1, A2, A3, n1, n2, β, α and Q.

$\ln(A_1)$	n_1/m	Q_1[KJ/mol]	$\ln(A_2)$	β[MPa^{-1}]	Q_2[kJ/mol]	α	$\ln(A_3)$	n_2	Q_3[kJ/mol]
8.2	1.49/0.67	184±8	11	0.09	188±10	0.06	12.3±2.5	1.08	187±8

2.4. Grain structure evolution at superplastic deformation

The microstructure evolution after superplastic deformation at a strain rate of 4×10^{-4} s−1 in a temperature range of 815–890 °C and a strain range of 0.4–1.6 was analysed by SEM to identify the causes of the strain hardening effect. The results of the quantities analysis of the grain size evolution

are shown in Fig. 7a, and the patterned microstructures in the longitudinal cross section after the strains of 0.7 and 1.6 at different temperatures are presented in Fig. 7b–f. The grain size insignificantly changes at 815 °C: α- and the β-grains grow from 3.6 to 5.1 μm and from 1.8 to 2.3 μm, respectively (blue lines in Fig. 7a). The average grains of both phases are fine at 840 °C, and there are no pronounced differences between the undeformed initial grain size and the grain size up to a strain of 0.6 (red lines in Fig. 7a). The average α- and β-grain sizes changed from 4.2 to 7.2 μm and from 2.2 to 4.2 μm, respectively, with an increase of the strain to 1.6 (400%). Some coarse grains are observed at 865 °C (green lines in Fig. 7a). A significant dynamic grain growth is found at 890 °C at the beginning of the superplastic deformation, and the grain size of both phases increases with an increase of the strain (black lines in Fig. 7a). The average dynamic grain growth rate of both phases increases almost in order from 3×10^{-4} μm/min to 1.3×10^{-3} μm/min with an increase of the temperature from 815 to 890 °C.
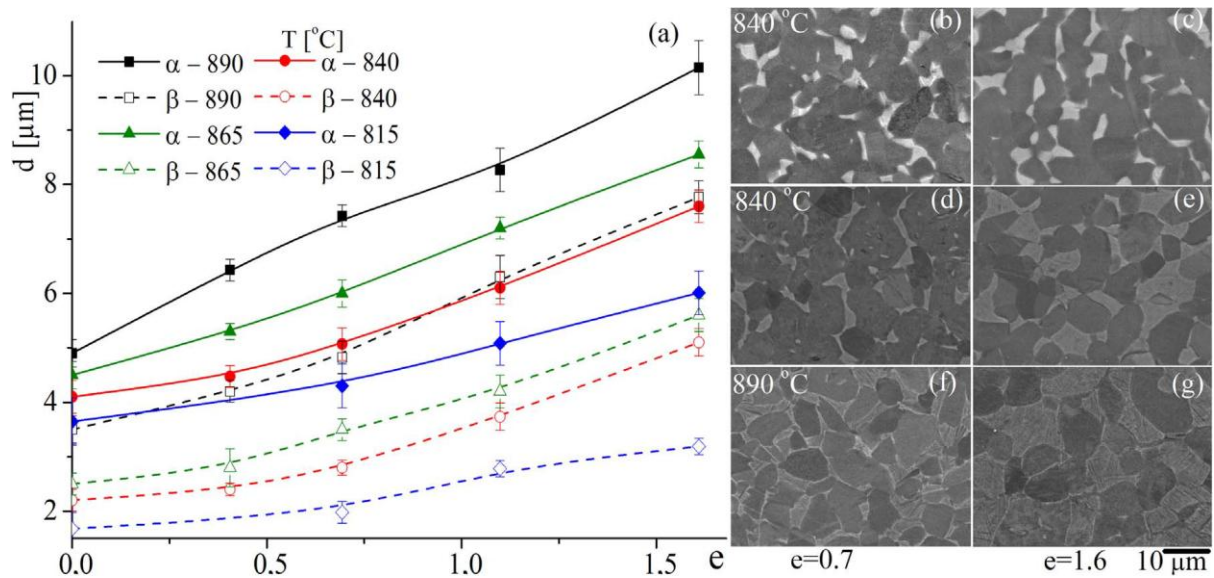

Fig. 7. The grain size vs the strain after superplastic deformation at 4×10^{-4} s−1 strain rate in a temperature range of 815–890 °C (a) and microstructures at 815 °C (b, c), 840 °C (d, e) and 890 °C (f, g) and strains of 0.7 (b, d, f) and 1.6 (c, e, g). (For interpretation of the references to color in this figure legend, the reader is referred to the web version of this article.)

Fig. 8 presents the electron backscatter diffraction (SEM-EBSD) grain-subgrain boundaries maps and the texture analysis of the as-annealed (time of 59 (a) and 97 min (b)) and the as-deformed (0.7 (c) and 1.6 (d) strain) samples at 840 °C. The time of 59 and 97 min of annealing corresponds with the strains of 0.7 and 1.6 at the strain rate of 4×10^{-4} s−1. It should be noted that the transformed β-phase exhibits the same HCP lattice as the α-phase at room temperature, and there are well as the average size of α and the transformed β-grains in the as-quenched sample. Thus, the grain size of the stable β-phase with the BCC lattice and the average grain size of both stable α-phase and α- phase

which can belong to β at the elevated temperatures are measured by a SEM-EBSD method. The volume fraction of the HCP phase (α and transformed β) is 95±1% and the BCC phase (stable β) is only 5±1% at room temperature, which corresponds with the volume fraction analysis of the initial microstructure as presented in Fig. 1. A strong texture is observed in the as-annealed conditions (Fig. 8a, b). For the as deformed conditions, the randomness of the crystal orientation increases with an increase of the strain; thus, the texture weakens as the superplastic strain accumulates (Fig. 8c, d).

The grain size of the β-phase varies from 1.9 to 2.5 μm, and there is no pronounced difference between the grain size after 0.7 and 1.6 strain; and after 59 and 97 min of annealing. Non-equiaxed shaped α- grains of 4.0 μm in size with high density (27%) of low-angle boundaries (LAB, green lines in Fig. 8a) are observed after 59 min of annealing with the deformed fraction (15%) of both phases (Fig. 8a). The recrystallisation process changes the structure to more equiaxed grains with a size of 4.5 μm. The LAB fraction decreases to 18% and the deformed fraction in both phases decreases to 4% after 97 min of annealing (Fig. 8b). The as-deformed samples exhibit mostly equiaxed α- grains with a size of 5.8 μm and 6.3 μm after 0.7 and 1.6 strains, respectively. The main misorientation angle is approximately 50°, and the fraction of the LAB boundaries is 10% (Fig. 8c and d). The deformed fraction increases to 55% in the stable β-phase at superplastic deformation.

Few free dislocations are observed by a TEM study in the α-phase after 97 min of annealing at 840 °C (Fig. 9a). Conversely, significant dislocation activities coupled with the formation of the dislocation walls inside the α-grains are observed after 0.7 (Fig. 9b) and 1.6 (Fig. 9c) strains. Analysis of the evolution of dislocation structure in the β-phase at superplastic deformation is difficult, because it is mainly the β-phase which exhibits polymorphic transformation when cooling to room temperature. The resulting changes in the dislocation structure are dependent on cooling conditions, polymorphic transformation and superplastic deformation.

The portion close to the failure zone of the sample tested at a temperature of 840 °C and the strain rate of 4×10^{-4} s^{-1} is shown in Fig. 10. Cavitation is not observed up to the failure of the sample (650% of strain). Mechanical properties at room temperature were studied in two conditions for comparison: as-deformed with 4×10^{-4} s^{-1} to strain of 0.7 (100%) and as-annealed after corresponding annealing time of 59 min. The samples were air cooled after both deformation and annealing. The yield stress (YS) of 540 MPa and the ultimate tensile strength (UTS) of 670 MPa as well as the yield stress of 490 MPa, and the ultimate tensile strength of 600 MPa are achieved in the as-annealed and the as-deformed states, respectively. Thus, both the YS and UTS decreased 10–12% as a result of superplastic deformation. The elongation is 14% in both states. It is notable that the conventional sheets of the near-α type alloys exhibit superplasticity at lower temperatures (up to 815 °C) as compared to the traditional Ti-6Al-4V alloy [2,21,22] with negligible cavitation and elongation of 600%, which is sufficient for successful application in the superplastic forming technology.
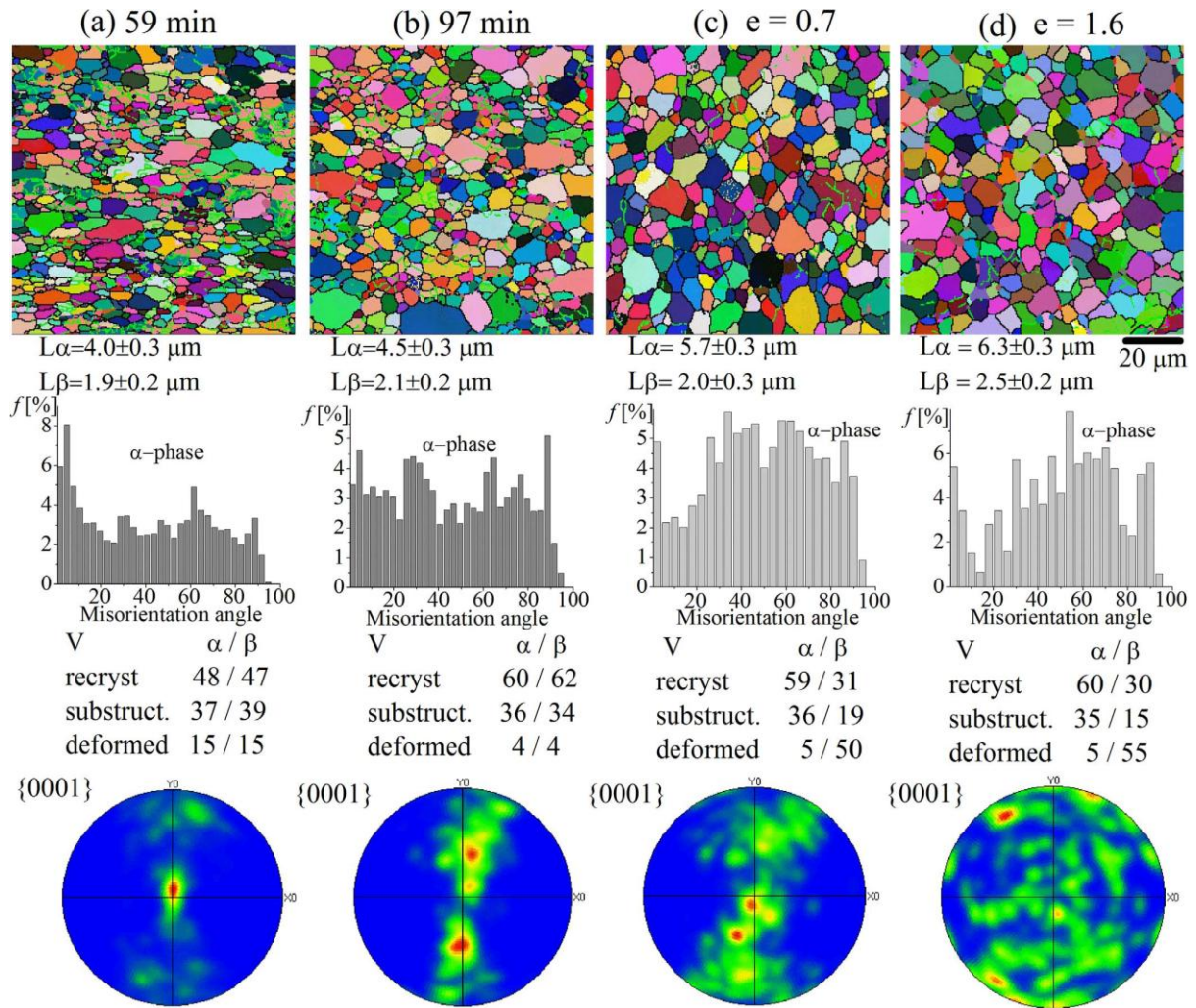
Fig. 8. The electron backscatter diffraction analysis and the estimated texture for the α-phase in Ti-2.5Al-1.8Mn titanium alloy after annealing of 59 (a) and 97 min (b) and after the tensile strain at 840 °C with a strain rate of 4×10^{-4} s^{-1} at different tensile stages: (a) e = 0.7 and (b) e = 1.6; black lines are high-angle boundaries and green lines are low-angle boundaries. (For interpretation of the references to color in this figure legend, the reader is referred to the web version of this article.)

3. Discussion

Theoretically, different processes can occur at superplastic deformation such as: (i) grain boundary sliding accommodated by dislocation slip/creep, diffusion creep and grain rotations [2,23–29], (ii) dynamic recovery and recrystallisation [11,13,17,29–36], and (iii) dynamic grain growth [37–39]. It is widely believed that grain boundary sliding is the main mechanism for superplasticity of Ti alloys, and grain boundary sliding is accommodated by diffusion creep and dislocation slip/creep or both [2,36,37,40–42]. Many structure parameters affect superplastic deformation behaviour due to their influence on the deformation mechanisms. It is known that the volume fraction and the grain size of

phases play a critical role in superplasticity of duplex type two-phase materials [2]. In particular, when a crystal structure of the phases is different — HCP for α and BCC for β — the phases exhibit different deformation behaviour and diffusion characteristics. It is known [29,43,44] that the BCC β is considerably softer than the α phase at elevated temperatures due to higher diffusivity and more slip systems of dislocations. The optimal superplastic temperature of two-phase materials like Ti 6-4 are usually observed when the volume fraction of the α/β phase is close to 50/50 [2] due to a low dynamic grain growth, high density of interphase boundaries which simplified the grain boundary sliding in the α/β boundaries [45–48] and a high amount of soft deformable β-phase which improves both intragranular mechanisms of superplastic deformation - dislocation and diffusion creep [2,29,49]. Thus, the volume fraction of the β-phase could play a critical role in the deformation mechanisms and the final superplastic properties of Ti alloys. In the studied alloy, the α/β = 50/50 temperature (T50/50) is close to 865 °C, according to the microstructural analysis and Thermocalc calculation. With the above in mind, the expected optimum superplasticity should be found at this temperature. On the contrary, the maximum elongation of 600–650% corresponding with the maximum m-values (Fig. 6e, f) are found in a temperature range of 815–850 °C, which belonged to the α+β field with 70–88% volume fraction of the α-phase and only 30–12% of the β-phase. The elongation decreased to 400% with increasing the temperature to T50/50 = 865 °C.
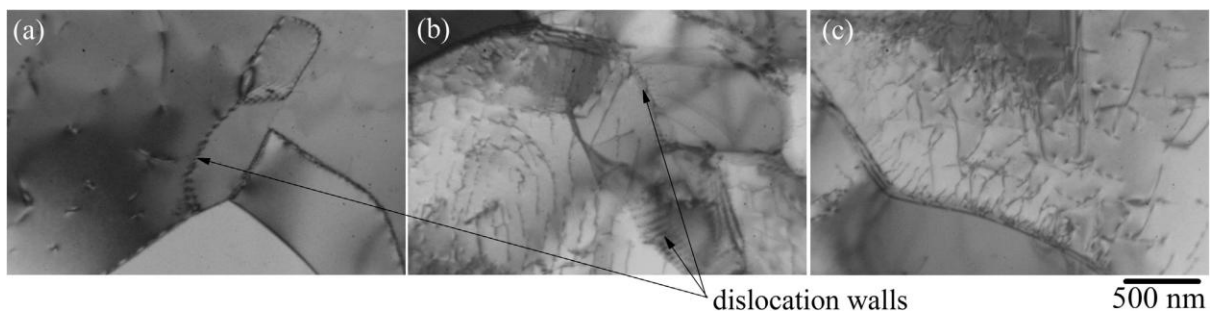

Fig. 9. TEM structure of the α-phase after 97 min of annealing (a) and after superplastic deformation with strains of 0.7 (b) and 1.6 (c)

The stress strain curves analysis showed that the strain hardening coefficient dramatically increases with an increase of the temperature from 815 to 865 °C, and especially to 890 °C, being mainly a result of the dynamic grain growth effect, which is in agreement with [13]. Thus, both the increasing strain hardening coefficient and the decreasing elongation values with an increase of the temperature are the results of the dynamic grain growth effect. Whiles the β-phase exhibits high diffusivity, it also undergoes a strong rapid grain growth at elevated temperatures. The additional possible reason for such a significant dynamic grain growth at ≥ T50/50 in the studied near-α alloy is the low solute content in the β-phase at elevated temperatures. The concentration of Mn in the β-phase strongly decreased from 4.5 to 1.5 wt% with an increase of the temperature from 815 to 890 °C. The composition of the α-phase slightly depends on temperature, but the concentration of the alloying

elements does not exceed 3 wt% (Fig. 3c). It is known that the α-phase significantly restricts the grain growth because of the long-range diffusion, which is necessary to transfer highly partitioned alloying elements, for example, vanadium in β phase in Ti 64. The concentration of V in the β-phase is comparatively high (6 wt%) at an optimum superplastic deformation temperature of 900 °C [21,22,37,38], according to the ThermoCalc calculation of the phase compositions of the Ti-6Al-4V alloy. The poorly alloyed β-phase in the studied near-α alloy can lose temperature stability due to changed diffusion characteristics and atomic diffusion mechanisms at high temperatures. Conversely, high solute content in the β-phase inhibits β-grains growth, and content of solute atoms additionally with temperature affects the grain stability. The same improvement of the superplasticity due to enhanced ductility of the heavily alloyed β-phase with the BCC lattice was observed in duplex type brass in [50]. The significant effect of solute content on the dynamic grain growth and superplastic behaviour in aluminium alloys was observed in [39,51,52]. Probably, superplastic deformation behaviour of two-phase materials with a duplex type structure depends on the phase composition at elevated temperatures in addition to the grain size and the volume fraction of the phases.
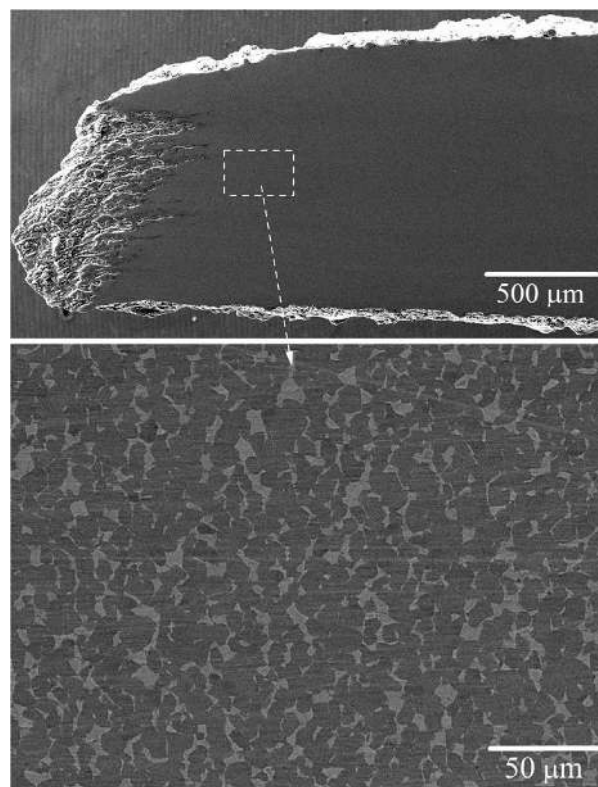

Fig. 10. Failure zone of the sample after 650% of strain at temperature of 840 °C and strain rate of 4 × 10−4 s−1

The studied alloy exhibits a lower fraction of the LAB and a more equiaxed grain shape after deformation as compared to the undeformed structure as a result of the EBSD studies (Fig. 8), a poligonisation process with high density of dislocations observed by TEM in as-deformed state. Thus,

the accumulation of dislocations at deformation increases the misorientation angle of the subgrain boundaries and supported the acceleration of the equiaxed grain structure formation. These observations at the initial stage of deformation are attributed to the dynamic recrystallisation effect. Both the YS and the UTS are lower in the asdeformed state with a strain of 0.7 as compared to the as-annealed state with corresponding annealing time of 59 min without any decrease in the elongation and cavitation. Decreasing mechanical strength at room temperature in the as-deformed state can also be attributed to dynamic recrystallisation. Dynamic recrystallisation is usually observed in materials with partially unrecrystallised or entirely banded grain structure before the start of superplastic deformation [39,53–57]. Several works [15–17] observed the dynamic recrystallisation effect at superplastic deformation in near-α Ti alloys and in Ti 64 at low temperature of 750 °C [39]. There were no obvious changes in either the grain aspect ratio or fractions of high angle boundaries at the steady stage of the superplastic flow of the studied alloy. In result, there is no recourse to suggest that there was dynamic recrystallisation at the steady stage of deformation. However, evidences of dynamic poligonisation are observed in the α-phase at large strains (Fig. 9b–d).

 The dominant mechanism of superplastic deformation at the steady stage could be suggested by the analysis of the effective activation energy of superplastic deformation and strain rate sensitivity index m. The activation energies have been reported for grain boundary selfdiffusion as 183 kJ mol−1 and 153 kJ mol−1; and for intragranular diffusion as 306 and 317 kJ mol−1 in α-Ti and β-Ti, respectively [58,59]. The effective activation energy of 184 kJ mol−1 are calculated in a temperature range of superplasticity from 815 to 890 °C. This value is close to the activation energy for the grain boundary self-diffusion in α-Ti and is significantly lower than the lattice self-diffusion of both phases. Such a value of the effective activation energy for superplastic deformation in Ti alloys is usually associated with the grain boundary sliding mechanism [60] accommodated by grain boundary diffusion [32]. Additionally, at strain rate sensitivity index m>0.5, the equiaxed shape of α-grains at the steady stage of deformation is retained. A significant weakening of the crystallographic texture at deformation is found, which is typical for grain boundary sliding controlled superplasticity in region II. These effects support the claim that the grain boundary sliding is the dominant mechanism, which is in agreement with a well-known description of superplastic phenomena [2].

High dislocation activity in the α-phase observed by TEM at superplastic flow shows that GBS in the α-grains is accommodated by a dislocation slip/creep mechanism. Dislocation activity in the ductile β-phase at superplastic deformation can be suggested according to the EBSD analysis which showed a significant increase in the deformed fraction of the β-grains. Evidences of plastic deformation in the β-phase with insignificant deformation in the α-phase appear at 900 °C for the Ti-6A1-4V alloy, as shown by Leader et al. [61]. Also, high dislocation activity in the β-phase at superplastic deformation was observed in-situ by Alabort [39]. Thus, the fine β-phase inhibits the dynamic α-grains growth in the optimum superplastic temperature range and provides the accommodation mechanisms (diffusion

and dislocation creep), and as a result, a stable flow stage without any significant strain hardening and cavitation are observed.

4. Summary

Microstructure evolution and deformation behaviour of conventional sheets of Ti-2.5Al-1.8Mn alloy were analysed in a temperature range of 790–915 °C and a strain rate range of 10^{-5} to 10^{-2} s^{-1} to identify the optimum superplastic deformation temperature and strain rate ranges. The superplastic behaviour with m>0.4 and elongation above 300% is observed in a temperature range of 815–890 °C and a strain rate range of 2×10^{-4} to 1×10^{-3} s^{-1}. Low strain hardening with n<0.2 is found at a temperature range of 815–850 °C, and n increases to n = 0.4 at 865–890 °C, which was explained by the dynamic grain growth effect. As shown by the SEM-EDS analysis, the concentration of Mn in the β phase significantly decreases with an increase of the temperature, and it is believed to be an additional factor for the dynamic grain growth acceleration which resulted in a decrease of the elongation values at high temperatures. As a result, the maximum elongation of 600–650% without cavitation is achieved at a temperature range of 815–850 °C and with the β volume fraction of 12–30%.

 It was found that the effective activation energy of superplastic deformation is 184–188 kJ/mol, and it can be associated with the domination of the grain boundary sliding mechanism between the α- grains. Grain boundary sliding in the α-grains is accommodated by a dislocation slip/creep mechanism, which is confirmed by a significant dislocation activity at superplastic flow at 840 °C and 4×10^{-4} s^{-1}. The dynamic recrystallisation effect which supported the formation of the equiaxed grain structure is observed at the initial stage of the deformation with a strain below 0.7. Poligonisation occurred in the α- phase at large strains of 0.7 and 1.6. It is assumed that fine and ductile β-phase decreases the dynamic grain growth effect in the α-phase, and simplifies the accommodation process of the superplastic deformation.

Acknowledgements

References

[1] V.N. Moiseyev, Titanium Alloys Russian Aircraft and Aerospace Applications, CRC Press, New York, 2005, p. 206, http://dx.doi.org/10.1201/9781420037678.

[2] T.G. Nieh, J. Wadsworth, O.D. Sherby, Superplasticity in Metals and Ceramics, Cambridge University Press, Cambridge, 1997, http://dx.doi.org/10.1017/CBO9780511525230.

[3] R.R. Boyer, Titanium for aerospace: rationale and applications, Adv. Perform. Mater. 2 (1995) 349–368, http://dx.doi.org/10.1007/BF00705316.

[4] D. Lee, W.A. Backofen, Superplasticity in some titanium and zirconium alloys, Trans. Met. Soc. AIME 239 (1967) 1034–1040.

[5] M. Motyka, J. Sieniawski, W. Ziaja, Microstructural aspects of superplasticity in Ti-6Al-4V alloy, Mater. Sci. Eng. A 599 (2014) 57–63, http://dx.doi.org/10.1016/j.msea.2014.01.067.

[6] A.V. Sergueeva, V.V. Stolyarov, R.Z. Valiev, A.K. Mukherjee, Enhanced superplasticity in a Ti-6Al-4V alloy processed by severe plastic deformation, Scr. Mater.43 (2000) 819–824, http://dx.doi.org/10.1016/s1359-6462(00)00496-6.

[7] Y.G. Ko, W.G. Kim, C.S. Lee, D.H. Shin, Microstructural influence on low-temperature superplasticity of ultrafine-grained Ti-6Al-4V alloy, Mater. Sci. Eng. A 410–411 (2005) 156–159, http://dx.doi.org/10.1016/j.msea.2005.08.080.

[8] S.A. Aksenov, E.N. Chumachenko, I.V. Logashina, Experimental investigation of Ti-Al-V alloy superplastic behavior, Metal 5 (2012) 3–8 http://publications.hse.ru/en/view/71848824.

[9] W. Jia, W. Zeng, H. Yu, Effect of aging on the tensile properties and microstructures of a near-alpha titanium alloy, J. Mater. 58 (2014) 108–115, http://dx.doi.org/10.1016/j.matdes.2014.01.063.

[10] X. Zhang, L. Cao, Y. Zhao, Y. Chen, X. Tian, J. Deng, Superplastic behavior and deformation mechanism of Ti600 alloy, Mater. Sci. Eng. A 560 (2013) 700–704, http://dx.doi.org/10.1016/j.msea.2012.10.016.

[11] X. Zhang, Y. Zhao, W. Zeng, Effect of hydrogen on the superplasticity of Ti600 alloy, Int. J. Hydrog. Energy 35 (2010) 4354–4360, http://dx.doi.org/10.1016/j.ijhydene.2010.01.110.

[12] Q.J. Sun, G.C. Wang, M.Q. Li, Enhanced the superplasticity in Ti-6.5Al-2Zr-1Mo-1V alloy by a two-step deformation method, Mater. Des. 35 (2012) 80–86, http://dx.doi.org/10.1016/j.matdes.2011.09.025.

[13] Q.J. Sun, G.C. Wang, Microstructure and superplasticity of TA15 alloy, Mater. Sci. Eng. A 606 (2014) 401–408, http://dx.doi.org/10.1016/j.msea.2014.03.117.

[14] Y.Q. Ning, B.C. Xie, M.W. Fu, H.Q. Liang, Z.K. Yao, H.Z. Guo, Microstructure and superplastic deformation for aerospace Ti-alloys associated with α-phase curing behavior, Aerosp. Sci. Technol. 45 (2015) 416–421, http://dx.doi.org/10.1016/j.ast.2015.06.010.

[15] P. Lin, A. Feng, S. Yuan, G. Li, J. Shen, Microstructure and texture evolution of a near-α titanium alloy during hot deformation, Mater. Sci. Eng. A 563 (2013) 16–20, http://dx.doi.org/10.1016/j.msea.2012.11.064.

[16] Z. Liu, P. Li, L. Xiong, T. Liu, L. He, High-temperature tensile deformation behaviour and microstructure evolution of Ti55 titanium alloy, Mater. Sci. Eng. A 680 (2017) 259–269, http://dx.doi.org/10.1016/j.msea.2016.10.095.

[17] Z. Liu, P. Li, L. Geng, T. Liu, H. Gao, Microstructure and texture evolution of TA32 titanium alloy during superplastic deformation, Mater. Sci. Eng.: A 699 (2017) 71–80, http://dx.doi.org/10.1016/j.msea.2017.05.082.

[18] X. Xu, G. Wang, C. Xia, Stepped superplasticity deformation-induced plastic enhancement of Ti-6Al-1.5Cr-2.5Mo-0.5Fe-0.3Si alloy, Mater. Des. 36 (2012) 136–140, http://dx.doi.org/10.1016/j.matdes.2011.09.048.

[19] C. Zener, J.H. Hollomon, Effect of strain rate upon plastic flow of steel, J. Appl. Phys. 15 (1944) 22–32, http://dx.doi.org/10.1063/1.1707363.

[20] C.M. Sellars, W.J. McTegart, On the mechanism of hot deformation, Acta Metall. 14 (1966) 1136–1138, http://dx.doi.org/10.1016/0001-6160(66)90207-0.

[21] E.N. Chumachenko, V.K. Portnoi, L. Paris, T. Billaudeau, Analysis of the SPF of a titanium alloy at lower temperatures, J. Mater. Process. Technol. 170 (2005) 448–456, http://dx.doi.org/10.1016/j.jmatprotec.2005.02.270.

[22] E. Alabort, D. Putman, R.C. Reed, Superplasticity in Ti-6A-4V: characterisation, modelling and applications, Acta Mater. 95 (2015) 428–442, http://dx.doi.org/10.1016/j.actamat.2015.04.056.

[23] A. Ball, M.M. Hutchinson, Superplasticity in the aluminum-zinc eutectoid, Met. Sci.J. 3 (1969) 1–7, http://dx.doi.org/10.1179/msc.1969.3.1.1.

[24] T.G. Langdon, Seventy-five years of superplasticity: historic developments and new opportunities, J. Mater. Sci. 44 (2009) 5998–6010, http://dx.doi.org/10.1007/s10853-009-3780-5.

[25] M.F. Ashby, R.A. Verrall, Diffusion-accommodated flow and superplasticity, Acta Metall. 21 (1973) 149–163, http://dx.doi.org/10.1016/0001-6160(73)90057-6.

[26] R.Z. Valiev, T.G. Langdon, An investigation of the role of intragranular dislocation strain in the superplastic Pb-62% Sn eutectic alloy, Acta Metall. Mater. 41 (1993) 949–954, http://dx.doi.org/10.1016/0956-7151(93)90029-R.

[27] M.J. Mayo, W.D. Nix, Direct observation of superplastic flow mechanism in tortion, Acta Metall. 37 (1989) 1121–1134, http://dx.doi.org/10.1016/0001-6160(89)90108-9.

[28] A.K. Ghosh, R. Raj, Grain size distribution effects in superplasticity, Acta Metall. 29 (1981) 607–616, http://dx.doi.org/10.1016/0001-6160(81)90142-5.

[29] E. Alabort, P. Kontis, D. Barba, K. Dragnevski, R.C. Reed, On the mechanisms of superplasticity in Ti-6Al-4V, Acta Mater. 105 (2016) 449–463, http://dx.doi.org/10.1016/j.actamat.2015.12.003.

[30] H. Zhang, B. Bai, D. Raabe, Superplastic martensitic Mn-Si-Cr-C steel with 900% elongation, Acta Mater. 59 (2011) 5787–5802, http://dx.doi.org/10.1016/j.actamat.2011.05.055.

[31] T. Rajagopalachary', V.V. Kutumbarao, Superplastic behaviour of a titanium alloy IMI685 under uniaxial compression, Scr. Mater. 35–3 (1996) 305–309, http://dx.doi.org/10.1016/1359-6462(96)00134-0.

[32] G.C. Wang, M.W. Fu, H.B. Dong, J. Lu, Q.J. Sun, C.X. Cao, Superplasticity deformation of Ti-6Al-2Zr-1Mo-1V induced by the cyclic change of strain-rate and MaxmSPD, J. Alloy. Compd. 491 (2010) 213–217, http://dx.doi.org/10.1016/j.jallcom.2009.11.046.

[33] H. Matsumoto, V. Velay, A. Chiba, Flow behavior and microstructure in Ti-6Al-4V alloy with an ultrafine-grained α-single phase microstructure during low-temperature- high-strain-rate superplasticity, Mater. Des. 66 (2015) 611–617, http://dx.doi.org/10.1016/j.matdes.2014.05.045.

[34] H. Zhang, L. Zhang, X. Cheng, L. Xu, B. Bai, Superplastic behavior during warm deformation of martensite in medium carbon steel, Scr. Mater. 62 (2010) 798–801, http://dx.doi.org/10.1016/j.scriptamat.2009.12.001.

[35] H. Zhang, K.G. Pradeep, S. Mandal, D. Ponge, P. Choi, C.C. Tasan, D. Raabe, Enhanced superplasticity in an Al-alloyed multicomponent Mn-Si-Cr-C steel, Acta Mater. 63 (2014) 232–244, http://dx.doi.org/10.1016/j.actamat.2013.10.034.

[36] R. Panicker, A.H. Chokshi, R.K. Mishra, R. Verma, P.E. Krajewski, Microstructural evolution and grain boundary sliding in a superplastic magnesium AZ31 alloy, Acta Mater. 57 (2009) 3683–3693, http://dx.doi.org/10.1016/j.actamat.2009.04.011.

[37] A.K. Ghosh, C.H. Hamilton, Mechanical behavior and hardening characteristics of a superplastic Ti-6AI-4V alloy, Metall. Trans. A 10 (1979) 699–706, http://dx.doi.org/10.1007/BF02658391.

[38] A. Arieli, B.J. Maclean, A.K. Mukherjee, The effect of strain and concurrent grain growth on the superplastic behavior of titanium 6Al-4V alloy, Res. Mech. 6 (1983), 131–159.

[39] K. Sotoudeh, P.S. Bate, Diffusion creep and superplasticity in aluminium alloys, Acta Mater. 58 (2010) 1909–1920, http://dx.doi.org/10.1016/j.actamat.2009.11.034.

[40] J.R. Spingarn, W.D. Nix, Diffusional creep and diffusionally accommodated grain rearrangement, Acta Metall. 26 (1978) 1389–1398, http://dx.doi.org/10.1016/0001-6160(78)90154-2.

[41] A. Geckinli, Grain boundary sliding model for superplastic deformation, Met. Sci. 17 (1983) 12–18, http://dx.doi.org/10.1179/030634583790427504.

[42] A. Arieli, A. Rosen, Superplastic deformation of Ti-6Al-4V alloy, Metall. Mater. Trans. A 8A (1977) 1591–1596, http://dx.doi.org/10.1007/BF02644864.

[43] M.L. Meier, A.K. Mukherjee, Consequences of using the average diffusivity in correlating the enhanced superplasticity of iron-modified Ti-6Al-4V, Scr. Metall. Mater. 25 (1991) 1471–1476, http://dx.doi.org/10.1016/0956-716X(91)90435-4.

[44] S.L. Semiatin, F. Montheillet, G. Shen, J.J. Jonas, Self-consistent modeling of the flow behavior of wrought alpha/beta titanium alloys under isothermal and nonisothermal hot-working conditions, Metall. Mater. Trans. A 33 (2002) 2719–2727, http://dx.doi.org/10.1007/s11661-002-0394-9.

[45] S. Hashimoto, F. Moriwaki, T. Mimaki, S. Miura, Sliding along the interphase boundary in austenitic/ferritic duplex stainless steel bicrystals, in: Proceedings of the 4th International Conference on Superplasticity in Advanced-Materials, The Japan Society for Research on Superplasticity, Osaka, Japan (ICSAM-1991), pp.23–32. ISBN-13: 978-4-990018429.

[46] A. Eberhardt, B. Baudelet, Interphase boundary sliding at high temperature in twophase (б/в)-brass bicrystals, Philos. Mag. A 41 (1980) 843–869, http://dx.doi.org/10.1080/01418618008243892.

[47] J.S. Kim, J.H. Kim, Y.T. Lee, C.G. Park, C.S. Lee, Microstructural analysis on boundary sliding and its accommodation mode during superplastic deformation of Ti-6Al-4V alloy, Mater. Sci. Eng.: A 263 (1999) 272–280, http://dx.doi.org/10.1016/S0921-5093(98)01157-5.

[48] S. Roy, S. Suwas, Enhanced superplasticity for (α+β)-hot rolled Ti-6Al-4V-0.1B alloy by means of dynamic globularization, Mater. Des. 58 (2014) 52–64, http://dx.doi.org/10.1016/j.matdes.2014.01.033.

[49] T. Seshacharyulu, S.C. Medeiros, W.G. Frazier, Y.V.R.K. Prasad, Microstructural mechanisms during hot working of commercial grade Ti-6Al-4V with lamellar starting structure, Mater. Sci. Eng. A 325 (2002) 112–125, http://dx.doi.org/10.1016/S0921-5093(01)01448-4.

[50] O.A. Yakovtseva, A.V. Mikhaylovskaya, A.V. Pozdniakov, A.D. Kotov, V.K. Portnoy, Superplastic deformation behaviour of aluminium containing brasses, Mater. Sci. Eng. A 674 (2016) 135–143, http://dx.doi.org/10.1016/j.msea.2016.07.053.

[51] K.B. Hyde, P.S. Bate, Dynamic grain growth in Al-6Ni: modelling and experiments, Acta Mater. 53 (2005) 4313–4321, http://dx.doi.org/10.1016/j.actamat.2005.05.029.

[52] A.D. Kotov, A.V. Mikhaylovskaya, V.K. Portnoy, Effect of the solid solution composition on the superplasticity characteristics of Al–Zn–Mg–Cu–Ni–Zr alloys, Phys. Met. Metallogr. 115 (2014) 730–735, http://dx.doi.org/10.1134/S0031918X14070047.

[53] P.S. Bate, F.J. Humphreys, N. Ridley, B. Zhang, Microstructure and texture evolution in the tension of superplastic Al–6Cu–0.4Zr, Acta Mater. 53 (2005) 3059–3069, http://dx.doi.org/10.1016/j.actamat.2005.03.019.

[54] K.B. Hyde, P.S. Bate, Dynamic grain growth in Al–6Ni: modelling and experiments, Acta Mater. 53 (2005) 4313–4321, http://dx.doi.org/10.1016/j.actamat.2005.05.029.

[55] A.D. Kotov, A.V. Mikhaylovskaya, M.S. Kishchik, A.A. Tsarkov, S.A. Aksenov, V.K. Portnoy, Superplasticity of high-strength Al-based alloys produced by thermomechanical treatment, J. Alloy. Compd. (2016), http://dx.doi.org/10.1016/j.jallcom.2016.07.045.

[56] A.V. Mikhaylovskaya, A.D. Kotov, A.V. Pozdniakov, V.K. Portnoy, A high-strength aluminium-based alloy with advanced superplasticity, J. Alloy. Compd. 599 (2014) 139–144, http://dx.doi.org/10.1016/j.jallcom.2014.02.061.

[57] A.V. Mikhaylovskaya, O.A. Yakovtseva, V.V. Cheverikin, A.D. Kotov, V.K. Portnoy, Superplastic behaviour of Al-Mg-Zn-Zr-Sc-based alloys at high strain rates, Mater. Sci. Eng. A 659 (2016) 225–233, http://dx.doi.org/10.1016/j.msea.2016.02.061.

[58] M.L. Meier, D.R. Lesuer, A.K. Mukherjee, The effects of the б/в phase proportion on the superplasticity of Ti-6Al-4V and iron-modified Ti-6Al-4V, Mater. Sci. Eng. A 154 (1992) 165–173, http://dx.doi.org/10.1016/0921-5093(92)90342-X.

[59] X. Ma, W. Zeng, F. Tian, Y. Zhou, Y. Sun, Optimization of hot process parameters of Ti–6.7Al–2Sn–2.2Zr–2.1Mo–1W–0.2Si alloy with lamellar starting microstructure based on the processing map, Mater. Sci. Eng. A 545 (2012) 132–138, http://dx.doi.org/10.1016/j.msea.2012.03.011.

[60] H.J. Frost, M.F. Ashby, Deformation Mechanism Maps: the Plasticity and Creep of Metals and Ceramics, Pergamon Press, New York, 1982, p. 166 (ISBN-13: 978-0080293370).

[61] J.R. Leader, D.F. Neal, C. Hammond, The effect of alloying additions on the superplastic properties of Ti-6%Al-4%V, Metall. Trans. A 17 (1986) 93–106, http://dx.doi.org/10.1007/BF02644445.